# Methods for Estimating Surface Water Storage Changes and Their Evaluations

SHUSEN WANG,[a] JUNHUA LI,[a] AND HAZEN A. J. RUSSELL[b]

[a] *Canada Centre for Remote Sensing, Natural Resources Canada, Ottawa, Ontario, Canada*
[b] *Geological Survey of Canada, Natural Resources Canada, Ottawa, Ontario, Canada*

(Manuscript received 16 June 2022, in final form 7 December 2022)

ABSTRACT: Developing effective methods for estimating regional-scale surface water storage change (ΔSW) has become increasingly important for water resources studies and environmental impact assessment. Three methods for estimating monthly ΔSW are proposed in this study, of which one is based on land surface runoff and two that use water body water budgets. Water areas observed by Landsat satellites for Canada's entire landmass are used for evaluation of the results. The surface runoff method achieved the least satisfactory results, with large errors in the cold season or dry regions. The two water-budget methods demonstrated significant improvements, particularly when water area dynamics is considered in the estimation of the water body water budget. The three methods performed consistently across different climate regions in the country and showed better correlations with observations over wet climate regions than over dry regions with poorly connected hydrological system. The results also showed the impact of glacier and permanent snow melts over the Rocky Mountains on basin-scale surface water dynamics. The methods and outputs from this study can be used for calibrating and validating hydrological and climate models, assessing climate change and human disturbance impacts on regional water resources, and filling the ΔSW data gaps in GRACE-based total water storage decompositions studies.

SIGNIFICANCE STATEMENT: The purpose of this study is to develop and evaluate methods for estimating regional-scale surface water storage change. This is important because information on surface water dynamics is limited for water resources studies and environmental impact assessment. Our study makes available two new methods which significantly improve on surface water storage estimation from the traditional runoff model. A guide on controls of surface water dynamics is provided for regions under various hydroclimate and physiographic–hydraulic conditions and reveals the influence of glacier melt on surface water variations.

KEYWORDS: Evaporation; Hydrology; Water budget/balance; Remote sensing; Satellite observations; Water resources

## 1. Introduction

Surface water is one component of the total terrestrial water storage (TWS) which also includes soil water, groundwater, snow, and ice, among others. The Gravity Recovery and Climate Experiment (GRACE) satellite mission and its follow-on mission (GRACE-FO) have been monitoring global TWS changes since 2002 by measuring temporal variations of Earth's gravity field (Tapley et al. 2004; Landerer et al. 2020). GRACE observations have provided invaluable datasets to study the TWS dynamics beyond small-scale studies based on in situ data (e.g., Long et al. 2015; Li et al. 2016; Wang and Li 2016; Rodell et al. 2018; Famiglietti and Ferguson 2021; Scanlon et al. 2021). One important application of the GRACE observations is to decompose TWS into its individual components to study their status, long-term trends, and interactions. In particular, estimating groundwater storage change by removing the changes from all other water components in the TWS has been extensively conducted to fill knowledge gaps in understanding the impacts of climate change and human activities on the groundwater resources for large aquifers over the world (e.g., Rodell et al. 2009; Tiwari et al. 2009; Scanlon et al. 2012; Voss et al. 2013; Famiglietti 2014; Joodaki et al. 2014; Richey et al. 2015; Chen et al. 2016; Long et al. 2020; Rateb et al. 2020; Shamsudduha and Taylor 2020; Fatolazadeh and Goïta 2022; Li and Wang 2022). The removals of soil water and snow water equivalent in available studies were mostly based on datasets from in situ observations or land surface model (LSM) outputs, notably a vast majority of them used the LSM outputs from GLDAS (Rodell et al. 2004).

Datasets for surface water storage change (ΔSW) are scarce, particularly at large regional scale. Most LSMs do not include explicit surface water simulations. Ground-based surface water monitoring networks in most countries are commonly restricted to selected water bodies such as large lakes and hydroelectric or irrigation reservoirs, and the spatial coverage is often far from adequate for determining ΔSW at large regional scales. In some regions of the world, ground-based surface water monitoring networks do not exist. Restrictions on data access in some countries further hinder the study of ΔSW using ground-based observations. Adding to the challenge, global information on surface water is very inconsistent across spatial scales and regions. For example, the estimates

Denotes content that is immediately available upon publication as open access.

Supplemental information related to this paper is available at the Journals Online website: https://doi.org/10.1175/JHM-D-22-0098.s1.

*Corresponding author*: Shusen Wang, shusen.wang@canada.ca

DOI: 10.1175/JHM-D-22-0098.1

for total world lakes varies widely, ranging from about $2 \times 10^6$ to $5 \times 10^6$ km$^2$ in surface area, and from about $166 \times 10^3$ to $275 \times 10^3$ km$^3$ in total volume (Lehner and Döll 2004; Downing et al. 2006; McDonald et al. 2012; Verpoorter et al. 2014; Messager et al. 2016). Moreover, these datasets pose large limitations in estimating ΔSW at subseasonal scales (e.g., the GRACE TWS monthly scale), as most of them gives static information and are not dynamic time series.

Satellite remote sensing has the potential to detect and monitor surface water dynamics. Satellites for terrestrial surface water area monitoring include those using multispectral optical sensors such as MODIS and Landsat (Tulbure and Broich 2013; Zhao and Gao 2018; Wang et al. 2020), and those using synthetic aperture radar (SAR) technologies such as *RADARSAT-2*, *Envisat*, and Sentinel-1 (Li and Wang 2015; Bartsch et al. 2012; Huang et al. 2018; Bonnema et al. 2022). Several regional and global datasets for surface water areas have been produced from satellite observations, such as the Global Inundation Extent from Multi-Satellite (GIEMS) dataset which quantified the monthly distribution of surface water extent at ~25-km sampling intervals using multiple-satellite observations (Prigent et al. 2007; Papa et al. 2010), the global areal extent and temporal variations of known reservoirs at 500-m spatial resolution using MODIS data (Khandelwal et al. 2017), and a number of global surface water datasets produced using the Landsat satellites at 30 m resolution (Pekel et al. 2016; Ogilvie et al. 2018; Zou et al. 2018; Jones 2019; Yao et al. 2019; Pickens et al. 2020). Satellites for inland surface water level retrievals include satellite laser altimetry, such as *ICESat-2* (Cooley et al. 2021; Luo et al. 2022), and radar altimetry such as *Envisat* and Sentinel-3 (Shu et al. 2020; Chen et al. 2021). Datasets derived from satellite altimetry for global surface water levels include the Database for Hydrological Time Series over Inland Waters (DAHITI; Schwatke et al. 2015), which provides water level time series for more than 780 lakes, reservoirs, rivers and wetlands; the Global Reservoirs and Lakes Monitor (G-REALM; Birkett et al. 2011), and the global water level dataset by Cooley et al. (2021), which quantified water level variability and derived storage changes for 227 386 water bodies from October 2018 to July 2020. The ΔSW can be determined by combining data from multispace missions for water areas and heights, such as in Frappart et al. (2015), Crétaux et al. (2011), Normandin et al. (2018), Busker et al. (2019), Li et al. (2019), and Hou et al. (2022).

From the perspective of GRACE-TWS decomposition which requires large-scale continuous coverage of ΔSW at a monthly time step, remote sensing faces a number of key challenges. Both optical and SAR data have limitations for retrieving surface area changes in winter when water bodies are frozen and covered by ice or snow. Satellite altimetry for water level monitoring of frozen water bodies is also a challenge (Shu et al. 2020). Even in summer, missing observations due to atmospheric contaminations (e.g., clouds) and other factors make it difficult to obtain full valid data coverages for a region at high temporal resolutions. Most of the satellite altimetry data are only available for recent years and are limited in both time and space due to wide spacing of the satellite altimetry tracks. Existing studies typically focused on large lakes and reservoirs, resulting in the oversight of small lentic water bodies which can play important roles in contributing to the overall regional ΔSW (Downing 2010; Smith et al. 2002). The accuracy of measurements is also a major concern in many circumstances. For example, for small lakes and rivers, the measurement errors are often at a magnitude of several decimeters or higher due to the surrounding land influence (Schwatke et al. 2015; Boergens et al. 2016; Bergeron et al. 2020), far exceeding the magnitudes of natural water level month-over-month changes (Cooley et al. 2021). Most of the optical satellites that have long data records and high temporal resolutions only have a moderate spatial resolution of 250–1000 m (e.g., MODIS, VIIRS, AVHRR), which is too coarse to detect the month-by-month shoreline changes of a water body.

Due to the limitations in obtaining large regional-scale and subseasonal datasets for ΔSW, the vast majority of investigations on GRACE-TWS decomposition have either neglected surface water component (completely or partially) (e.g., Rodell et al. 2007, 2009; Richey et al. 2015; Xia et al. 2017) or used land surface runoff from LSMs as a proxy for ΔSW (e.g., Bhanja et al. 2016; Getirana et al. 2017; Thomas et al. 2017; Shamsudduha and Taylor 2020). The impact of ignoring surface water on TWS decomposition or the validity of surrogating ΔSW by surface runoff has rarely been examined, although some studies have demonstrated the important role of ΔSW in the TWS change (Kim et al. 2009; Getirana et al. 2017; Papa et al. 2013; Pokhrel et al. 2013; Salameh et al. 2017). Thus, developing effective methods for estimating regional-scale ΔSW and evaluating its dynamics have become of increasing interest for improving GRACE-TWS decomposition studies (Scanlon et al. 2019).

The objective of this study is to develop methods for ΔSW estimation. Two new methods are presented that are based on water body water budgets, one using constant water areas and the other being implemented with dynamic water area simulation. The results from these two new methods as well as the land surface runoff method are evaluated using Landsat-observed monthly water area variations. The study region for method evaluation is the Canadian landmass, an area that contains 62% of the world's total number of lakes and 32% of the world total terrestrial water area. Besides the significance of surface water in the total terrestrial water storage, the surface water process over the Canadian landmass is also highly complex due to the seasonal cycles of snow accumulation and melt, and water body freeze and thaw. Results from the two new methods showed a large improvement over the estimation by surface runoff. The methods are simple and can be easily implemented to fill the ΔSW data gaps in GRACE TWS decomposition studies. The methods and outputs can be used for calibrating and validating hydrological and climate models and for assessing climate change and human disturbance impacts on regional water resources. A list of acronyms is given in Table 1.

## 2. Materials and methods

### a. Methods

Three methods were used in the surface water storage change estimation: (i) runoff method, (ii) water budget with

TABLE 1. Nomenclature.

| | |
|---|---|
| ΔSW | Surface water storage change in depth of water with base area of study basin |
| $\Delta V$ | Water storage change by volume |
| $A_{\text{basin}}$ | Total area of a basin |
| $A_w$ | Surface water area in a basin |
| $C_G$ | Water retention capacity of ground surface |
| $D$ | Water deficit of a water body |
| $E$ | Water surface evaporation or ice/snow sublimation for frozen water bodies |
| EALCO | Ecological Assimilation of Land and Climate Observations model |
| $E_G$ | Evaporation of water on ground surface before water infiltrates or runs off |
| $I_G$ | Ground surface water infiltration |
| MDA | Major drainage areas |
| $P_w$ | Precipitation (including snow) directly received by water bodies |
| $Q$ | Land surface runoff |
| $R_G$ | Rain throughfall received on the ground surface |
| $S_{\text{melt}}$ | Water from snowmelt |
| WBDA | Water budget with dynamic water area method |
| WBSA | Water budget with static water area method |
| $W_{\text{dew}}$ | Dew formed on ground surface |
| $W_{\text{in}}$ | Water input into a water body |
| $W_{\text{input}}$ | Other types of water inputs such as irrigation |
| WNHB | Western and North Hudson Bay Major Drainage Area |
| $W_{\text{out}}$ | Water outflow of a basin |
| $\theta$ | Surrounding terrain slope of a water body |

static water area (WBSA), and (iii) dynamic water area simulations based on WBSA (WBDA). The three methods each employ additional enhanced data input to refine the storage change and reduce uncertainty. After the time series of monthly ΔSW were estimated, the ΔSW was adjusted by its minimum value as the baseline (so the final ΔSW values cannot be negative) in order to be evaluated with Landsat observations. All the water variables presented below refer to the water depth (mm) with a base area of the entire basin and at monthly time step.

The runoff method uses land surface runoff ($Q$) as a proxy for ΔSW. It basically assumes $Q$ produces a positive ΔSW causing water levels to rise in the network. In this study, the surface runoff generated by the land surface model EALCO [Ecological Assimilation of Land and Climate Observations, Natural Resources Canada; see section 2c(1)] was used. Land surface runoff in EALCO is simulated by the liquid water budget of the ground surface:

$$\Delta\text{SW} = Q = \max(0.0,\ R_G + S_{\text{melt}} + W_{\text{dew}} + W_{\text{input}} - I_G - C_G - E_G), \quad (1)$$

where $R_G$ is the rain throughfall received on the ground surface which is mainly determined by the difference between liquid precipitation and canopy interception, $S_{\text{melt}}$ is water from snowmelt, $W_{\text{dew}}$ is dew formed on the ground surface, $W_{\text{input}}$ is other types of water inputs such as irrigation, $I_G$ is ground surface infiltration, $C_G$ is the water retention capacity of ground surface under which water is temporally held by the ground surface for infiltration before the water flows away as surface runoff, and $E_G$ is evaporation of water before it infiltrates or runs off. All the above variables are obtained for each time step at 30 min and then upscaled to monthly values in this study.

When $Q$ is used as a proxy for ΔSW (e.g., in GRACE-TWS decomposition), it implicitly assumes that all the water from $Q$ is a surplus, so the ΔSW from the runoff method will never be below 0. This could be problematic in dry periods when water storage of a water body is in deficit conditions. Furthermore, since GRACE-TWS has a monthly time step, the runoff method essentially assumes that it takes one month for the $Q$ to flow out of the basin. Note that Eq. (1) only accounts for the liquid form of water, as precipitation in the form of snow will stay in the system and commonly has been accounted for separately in GRACE-TWS decomposition studies.

The second method, the WBSA method, is based on a simple surface water budget for water bodies in a basin:

$$\Delta\text{SW}_m = W_{\text{in},m} + D_{m-1} + f_w, \quad (2)$$

where $m$ denotes month, $W_{\text{in},m}$ is water input into the water bodies, $D_{m-1}$ is the water deficit of water bodies historically accumulated until the previous month (it cannot be above 0), $f_w$ is used to account for impact of the possible mismatch of actual water outflow time versus the monthly time step of the data used in this study on the ΔSW. The $W_{\text{in},m}$ is calculated as

$$W_{\text{in},m} = [A_w(P_{w,m} - E_m) + (A_{\text{basin}} - A_w)Q_m]/A_{\text{basin}}, \quad (3)$$

where $A_w$ is the surface water area in the basin and it is parameterized as a constant, $A_{\text{basin}}$ is the total area of the basin, $P_{w,m}$ is the precipitation (including snow) directly received by water bodies, $E_m$ is water surface evaporation or ice/snow sublimation for frozen water bodies, and $Q_m$ is calculated in Eq. (1). Note that snowfall on water bodies is added to the surface water storage directly, unlike that on land surface aforementioned. Because snowfall is accounted for in the month when it occurs, the springtime melt of accumulated snow in the winter season on the frozen water body surface will not change the ΔSW at that time. Essentially, the $W_{\text{in},m}$ is composed of two parts: the first part represents the water body water yield, or the net water exchange between water bodies and the atmosphere, and the second part represents the water input from surrounding land surface to the water bodies.

When $W_{\text{in},m}$ in month m is negative, water bodies have net water loss and it contributes to the water deficit ($D$) of water bodies. This addresses the limitation in the Runoff method mentioned above. When $W_{\text{in},m}$ is positive, the water will first replenish the water bodies until water deficit $D$ reaches zero [Eq. (4)]. After that, any available water is treated as a surplus and will flow out of the system ($W_{\text{out}}$) [Eq. (5)]:

$$D_m = \min(W_{\text{in},m} + D_{m-1},\ 0.0), \quad (4)$$

$$W_{\text{out},m} = \max(W_{\text{in},m} + D_{m-1},\ 0.0). \quad (5)$$

TABLE 2. Major drainage areas (MDAs) and lake distributions in Canada (MDAs are from Statistics Canada 2003). Number of lakes and area of lakes are calculated using the HydroLAKES database (https://www.hydrosheds.org/products/hydrolakes, last access 31 March 2022; Messager et al. 2016). Data refer to all natural lakes and manmade reservoirs with a surface area ≥ 0.1 km$^2$. Transboundary lakes are assigned to only one MDA based on the maximum area. The Great Lakes of North America are not included; data for all of Canada are shown in bold in the last row.

| | | Number of lakes | | Area of lakes | |
|---|---|---|---|---|---|
| MDA name | MDA area (km$^2$) | Total | Per $10^3$ km$^2$ land | Size (km$^2$) | Percent |
| 1) Maritime Provinces | 163 990 | 3963 | 24.2 | 4602 | 2.8% |
| 2) St. Lawrence | 1 067 879 | 85 580 | 80.1 | 74 760 | 7.0% |
| 3) Northern Quebec and Labrador | 1 158 292 | 167 041 | 144.2 | 162 148 | 14.0% |
| 4) Southwestern Hudson Bay | 735 320 | 55 734 | 75.8 | 50 914 | 6.9% |
| 5) Nelson River | 987 015 | 33 278 | 33.7 | 89 767 | 9.1% |
| 6) Western and Northern Hudson Bay | 1 253 213 | 196 847 | 157.1 | 186 153 | 14.9% |
| 7) Great Slave Lake | 974 853 | 76 439 | 78.4 | 108 660 | 11.1% |
| 8) Pacific | 666 349 | 11 348 | 17.0 | 15 282 | 2.3% |
| 9) Yukon River | 337 036 | 5954 | 17.7 | 6588 | 2.0% |
| 10) Arctic | 2 605 138 | 243 310 | 93.4 | 188 364 | 7.2% |
| 11) Mississippi River | 27 097 | 174 | 6.4 | 199 | 0.7% |
| **Canada** | **9 976 182** | **879 668** | **88.2** | **887 438** | **8.9%** |

The term $f_w$ in Eq. (2) is calculated as

$$f_w = -\beta W_{\text{out},m} + (1.0 - \beta)^2 W_{\text{out},m-1}, \quad 0 < \beta < 1. \tag{6}$$

The time for the surplus water to flow out of the system depends on the geographic nature of a basin (e.g., basin size, slope, drainage network density) (Allen et al. 2018). By comparing the time difference between peak snowmelt and the peak river flow induced by the snowmelt, Wang and Russell (2016) and Wang et al. (2017) estimated the water outflow time to be about two weeks for the Red River basin and over three weeks for the Makenzie River basin in Canada. The Red River basin has a flatter terrain but a smaller drainage area ($116 \times 10^3$ km$^2$), compared with the Mackenzie River basin having a rougher terrain and the largest area and longest river in Canada ($1.8 \times 10^6$ km$^2$). The basins in this study (section 2b) vary greatly in size, terrain topography, and hydrological drainage connections, which could result in very different water outflow time. To compensate for any mismatch with the data time step of one month in this study, the above adjustment is necessary. For the two extreme cases, a $\beta$ value of 1.0 suggests that the time for the surplus water to flow out of the system is 0.0, which means the surplus water will not have any impact on the ΔSW, and a $\beta$ value of 0.0 suggests that it would take two months for the surplus water to flow out of the system, so the surplus water will stay in the system and contribute to the ΔSW for two consecutive months. Without $f_w$ the method essentially assumes that the surplus water stays in the system for one full month, but immediately leaves the system at the month end without affecting the ΔSW for the next month. The actual values for $\beta$ in this study was obtained through model best fitting with observed water areas from the Landsat satellites [section 2c(3)].

The third method, the WBDA method, is based on WBSA, but with dynamic water area simulations. When surface water storage changes, the surface area $A_w$ in Eq. (3) is likely to change accordingly, which will affect the water budget of the water bodies. For example, assuming an inverted-cone-shaped lake with a surface area of $S_0$ and a surrounding terrain slope of $\theta$ [tan($\theta$) = height difference/horizontal distance], a water storage change of $\Delta V$ by volume will result in a surface area change of $\Delta S$ [Eq. (7)]:

$$\Delta S = [S_0^{3/2} + 3\Delta V\sqrt{\pi}/\tan(\theta)]^{2/3} - S_0. \tag{7}$$

In this study, we used the above simple case to estimate the area variations with water storage changes. The $S_0$ was parameterized using the average size of lakes in a basin (Table 2). Rivers and small water bodies of less than 0.1 km$^2$ are not included in the HydroLAKES database, so they are not reflected in our parameterization. For specific watershed studies, the $S_0$ can be parameterized more accurately using known water body sizes. Note that the average size rather than the total size of lakes is used in the parameterization, as the latter case could deviate more significantly from the actual $\Delta S$–$\Delta V$ relationships for a basin with large number of lakes such as in our study. The $\Delta V$ is the water storage change (by volume) obtained in Eq. (2) for each time step. The $\theta$ was obtained through best fitting the time series of simulated surface water areas with the Landsat-observed surface water areas.

While the WBDA method can simulate the dynamic change of water areas which can be directly compared with the water area from the Landsat data, the Runoff and WBSA methods only give estimates for surface water storage changes which have a dimension of length $L^3$. To evaluate their results using Landsat data, we converted their storage estimates into a virtual area variable $(\Delta\text{SW} \times A_{\text{basin}})^{2/3}$. This virtual variable has a dimension $L^2$ (area), and is used to represent the relative area variations and compare with the Landsat data. The WBSA and WBDA methods do not include the impact of direct lake–aquifer water exchanges on the water budget. Its impact on the ΔSW estimation will be discussed later in the paper.


FIG. 1. Map of the 11 studied basins [the major drainage areas (MDAs) in the Standard Drainage Area Classification (SDAC; Statistics Canada 2003)].

*b. Study region*

The study region covers Canada's entire landmass. It includes 11 drainage basins which are termed as "major drainage areas" (MDAs; Fig. 1) in the Standard Drainage Area Classification (SDAC; Statistics Canada 2003). The MDAs provide a hydrological unit for data collection and compilation, and for spatial analysis of environmental, economic, and social statistics. They will be used in this study for presenting the results. The hydroclimate conditions have large variations across the Canadian landmass. Precipitation decreases from over 1000 mm $yr^{-1}$ in the west and east coasts to under 300 mm $yr^{-1}$ in the western interior lowlands and the high Arctic (Wang et al. 2013). Water surface evaporation increases from under 200 mm $yr^{-1}$ in the north to over 1000 mm $yr^{-1}$ in the southwest prairies (Li et al. 2020). Land surface evapotranspiration varies from 600 mm $yr^{-1}$ over several regions in the south to less than 100 mm $yr^{-1}$ in the northern Arctic (Wang et al. 2013; Fernandes et al. 2007). As a result, land surface water yield has a large decrease from over 800 mm $yr^{-1}$ in the west and east coasts to basically 0 in the southwest prairies (Li and Wang 2021), and water body water yield varies in a range from over 800 mm $yr^{-1}$ in the west coast to $-600$ mm $yr^{-1}$ in the southwest prairies.

Surface geology and climate govern the nature and distribution of water bodies in the Canadian landmass. There are around 880 000 natural lakes with a surface area of over 10 ha distributed over Canada's landmass (Minns et al. 2008; Messager et al. 2016), which account for 62% of the world total number of lakes. The total area of these lakes is about $856.5 \times 10^3$ $km^2$, which accounts for 32% of the total area of world lakes. Many Canadian lakes are distributed through a 1000-km swath of land surrounding Hudson Bay (Fig. 2). Nearly all of them are of glacial origin. The line of contact between the Canadian Shield and the western interior lowlands is marked by a band of Canada's largest lakes, ranging from Great Bear Lake in the Northwest Territories to the Laurentian Great Lakes of North America (Fig. 2). Table 2 lists the lake total numbers and areas in each MDA. Note that the above estimates do not include the Laurentian Great Lakes of North America, which are the largest group of freshwater lakes on Earth with a total area of over $244 \times 10^3$ $km^2$. Additionally, these estimates only include natural lakes and manmade reservoirs of over 10 ha and do not include rivers and small water bodies under 10 ha. Given the enormous number of small water bodies over the landmass (Messager et al. 2016), the actual total lake numbers and surface water areas are expected to be significantly higher than our estimates.

*c. Datasets*

Three main datasets were used in this study: land surface runoff, water body water yield, and water surface areas. Details for these datasets are given below.

1) LAND SURFACE RUNOFF ($Q$)

Land surface runoff was generated using the land surface model EALCO V4.2 (Wang et al. 2013). EALCO is developed

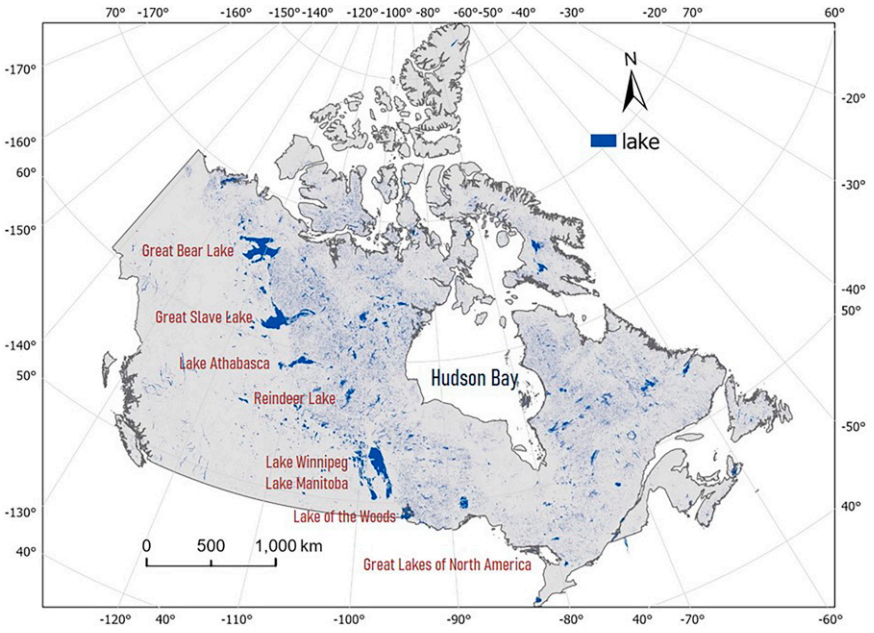


FIG. 2. Lakes (>0.1 km$^2$) over Canada's landmass show in dark blue. Note the outline of the Laurentia Great Lakes is not shown.

for simulating terrestrial ecosystem–atmosphere interactions using in situ and remote sensing observations. The model includes five main modules for simulating the dynamic land surface processes of radiation transfer at multiwavelengths (Wang et al. 2007), water transfer in the aquifer–soil–vegetation–atmosphere system (Wang 2008), canopy and ground surface energy balances (Wang et al. 2009; Zhang et al. 2008), and vegetation and soil carbon and nitrogen biogeochemical cycles (Wang et al. 2002). The water module is dynamically coupled with the other four modules in EALCO to integrate the controls of atmosphere, plant, and soil conditions in the ecosystem water cycle. Land surface runoff is obtained in the water module which simulates all the water processes described in Eq. (1). EALCO is developed in Canada with a specific focus on cold-region processes, such as soil freeze–thaw, snow accumulation and melt which include snow cover dynamic layering, compaction, destructive metamorphism, and surface albedo changes due to snow aging and surface littering (Zhang et al. 2008).

Evaluations of EALCO performances have been conducted for diverse ecosystems and climate conditions at various spatiotemporal scales. This includes model intercomparison [e.g., with the Community Land Model (CLM) and the Variable Infiltration Capacity (VIC) model of GLDAS], remote sensing products, watershed water budget, and in situ tower flux measurements (e.g., Hanson et al. 2004; Grant et al. 2006; Fernandes et al. 2007; Walker et al. 2014; Medlyn et al. 2015; Wang et al. 2015a; Chen et al. 2019). Recent assessments of EALCO water outputs over Canada's landmass include examining the monthly water budget closures for all gauged large drainage basins using GRACE observations, and the long-term (30 years) water budget closures for all gauged watersheds (Wang et al. 2014a,b, 2015b). The extensive tests and evaluations of EALCO over Canada's landmass have improved EALCO's algorithms and calibration and enhanced its performance particularly for cold region ecosystems, which provides confidence for model results of this study over the Canadian landmass.

The EALCO model in this study was driven by the atmospheric forcing produced by the Terrestrial Hydrology Research Group at Princeton University (Sheffield et al. 2006), which includes shortwave and longwave radiation, air temperature and humidity, precipitation, wind speed, and atmospheric pressure. It was parameterized by the remotely sensed land surface vegetation data and inventory soil maps (Wang et al. 2013). The simulated land surface runoff is provided at a 5-km spatial resolution and 30-min time step, and covering a time period of 38 years (1979–2016). The model outputs were then upscaled into monthly values for each of the MDAs. Note that all the variables in Eq. (1) and $P$ and $E$ in Eq. (3) were calculated at pixel-level first using subpixel information (Wang et al. 2013), before they were upscaled to the MDAs.

### 2) WATER BODY WATER YIELD ($P - E$)

Water body water yield refers to the net water exchange between water bodies and the atmosphere, or the difference between precipitation ($P_w$) and water body surface evaporation ($E$). The water yield dataset used in this study was detailed in Li and Wang (2021), in which the dataset was evaluated in Budyko space and compared with streamflow observations across Canada. The precipitation dataset in the water yield used that from Sheffield et al. (2006). It was constructed by combining a suite of global observation-based precipitation datasets with atmospheric model reanalysis and available globally at 0.25°. Later updates in the dataset can

found in http://hydrology.princeton.edu/data/pgf/v3/ (last accessed on 31 March 2022). Biases in the reanalysis precipitation were corrected using observation-based datasets. Corrections were also made to the rain day statistics of the reanalysis precipitation, which have been found to exhibit a spurious wave-like pattern in wintertime at high latitudes. This dataset provides long-term, spatially consistent precipitation and has been noted to be one of the most suitable datasets for studying land surface hydrology for long time periods and broad scales (Wang et al. 2013, 2014a).

Water surface evaporation ($E$) refers to the water loss to the atmosphere on the water body surface. In cold regions, the year-round estimation of $E$ is complicated by the water body freezing–thaw cycles, the associated ice–surface snow accumulation and melt, and the dynamic change of snow albedo that affects the snow surface energy balance. The $E$ used in the water yield calculation was produced by EALCO, which integrates the dynamic evolutions of water–ice–snow processes of water bodies into the estimation of $E$ (Li et al. 2020). The $E$ datasets demonstrated its high confidence levels through comparing with all the pan evaporation observations available in Canada in 1979–2007 (Li et al. 2020). It is so far the only available long-term $E$ dataset covering Canada's entire landmass that accounts for the dynamic water bodies surface changes (water–ice–snow) in $E$ calculations.

#### 3) SURFACE WATER AREA ($AW$)

The Global Surface Water (GSW) Monthly Water History product (https://jeodpp.jrc.ec.europa.eu/ftp/jrc-opendata/GSWE/MonthlyHistory/, last access 31 March 2022) generated using *Landsat-5*, *Landsat -7*, and *Landsat -8* archived data is used in this study. GSW applies an expert system for water extraction at 30 m resolution from over 4 000 000 Landsat scenes since 1984 (Pekel et al. 2016). To fully cover Canada's entire landmass, 33 tiles of this product were required, with each tile covering a $10° \times 10°$ region. A total number of 11 880 tiles for the period of 1991–2020 were used in this study, which provides an overlap of 26 years with the EALCO outputs. Validation of the GSW dataset for the period of 1984–2015 was performed by Pekel et al. (2016) using a total of 40 124 control points. Errors of omission overall were reported $<5\%$ and errors of commission $<1\%$. Our assessment of the dataset over the Canadian landmass generally confirmed this accuracy. Misclassification of water as land for pixels affected by missing observation of *Landsat-7* Scan Line Corrector (SLC)-off and cloud, however, became more significant in the dataset after September 2015 over the entire landmass, as illustrated in Fig S1 in the online supplemental material using the Arctic MDA as an example.

To estimate the actual water areas for each month in a MDA, we developed a Landsat data processing model. First, a permanent and inundation water mask was generated using all the monthly data for the 30 years of 1991–2020. It provides the base surface water areas information. Next, the water areas within the inundation areas for each month were calculated using the spatial and temporal coherence of the water pixels. Finally, the surface water area was obtained by adding the permanent water area for the region to the water area in the inundation area obtained above. This data processing method enables monthly water areas to be obtained, unless the no-data percentage in a region exceeds a threshold (95%) in a specific month. Moreover, it removes the misclassified pixels over the permanent water area and reduces the impact of misclassification errors on the estimation of water area over the inundation area due to the offset of commission errors and omission errors in the water–land ratio calculations. Figure S2 is an illustrative example, showing a GSW original product which contains substantial no-data and misclassified land pixels over Lake Amisk for September 2016 (left) and the postprocessed product from our data processing (right).

Due to the frozen water surface and snow cover conditions of the water bodies in winter, Landsat-based surface water areas had no data for the freeze-up period. The number of months with available data in a year varied from about 3–4 months for the Arctic MDA to 7–8 months for the Mississippi River, Maritime Provinces, and Pacific MDAs. Fortunately, the surface water changes in winter season are relatively small which reduces the impact of the Landsat data gaps in our evaluation.

## 3. Results

The surface water storage changes estimated by the three methods of runoff, WBSA, and WBDA are presented below. The Western and North Hudson Bay (WNHB) MDA, which has the highest lake distribution density (157.1 lakes per 1000 $km^2$), and the Mississippi River MDA, which is located in the driest region in Canada and has the lowest lake distribution density (6.4 lakes per 1000 $km^2$), are used to demonstrate the results. The results for all MDAs are summarized later in this section.

### *a. Land surface runoff method (runoff)*

The surface water storage variations estimated by the land surface runoff is shown in Fig. 3. For WNHB (Fig. 3a), surface water storage in winter months had the minimum value of 0 mm, as there was no land surface runoff modeled for WNHB when it was dominated by snow cover accumulation process and rain events rarely occur. In spring months, the surface water storage had a huge increase and reached its annual peak (42.6 mm) in June due to snowmelt-induced surface runoff. Low soil infiltration capacity due to the frozen soil in early spring also contributed to this large surface runoff. The surface water storage then had a sharp decrease and reached its lowest summer-season value in July (6.3 mm), mainly due to the large increase in soil infiltration capacity, a result of relatively dry soil from high evapotranspiration. The surface water storage had a slight increase after July until the cold season started in October, resulting in a second peak in September but with a much lower value (10.3 mm) than the spring peak. This is a time period with a large decrease in evapotranspiration and an increase in land water yield. Interannually, the standard variation of surface water storage in the 38 years had a maximum value of 11.0 mm observed in June. The coefficient of variation (CV = standard variation/mean) was observed to have a maximum value of 62% in July.

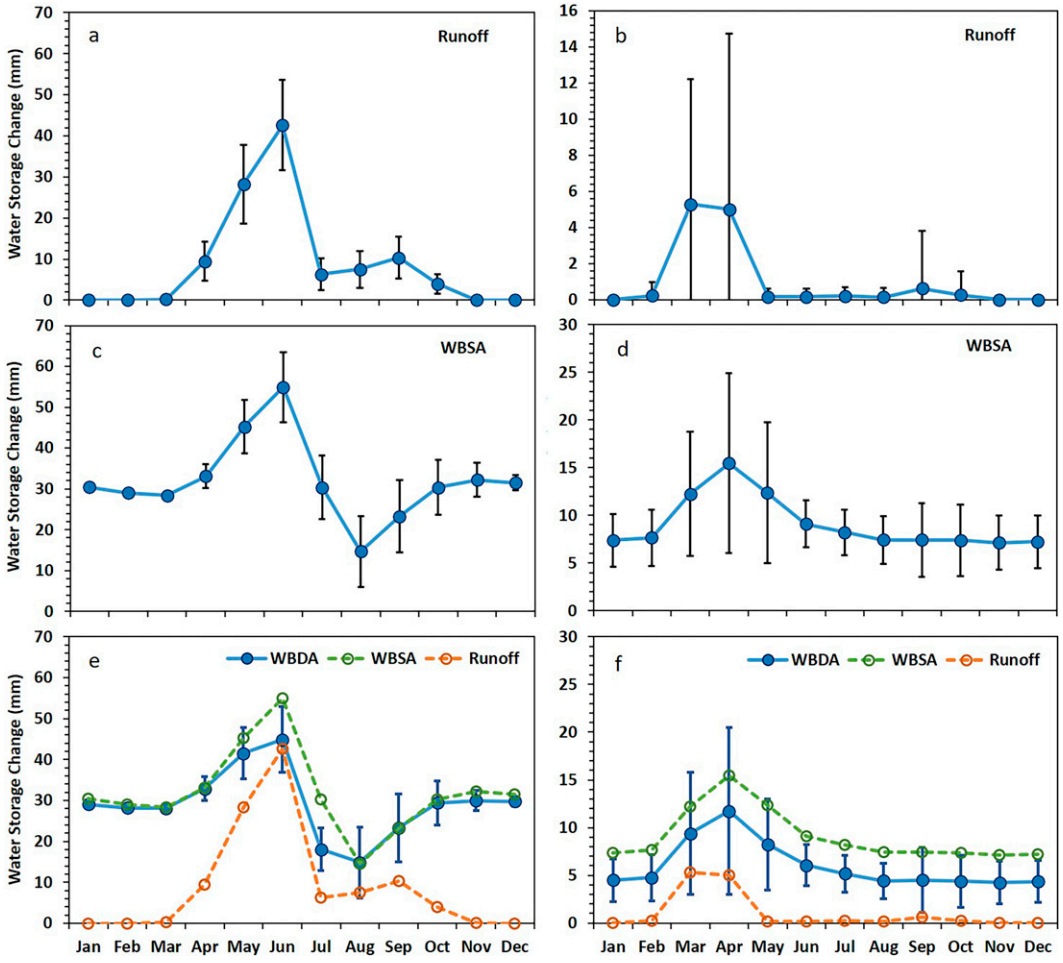


FIG. 3. Surface water storage change estimated for (left) the Western and North Hudson Bay MDA and (right) the Mississippi River MDA by the three methods of (a),(b) runoff, (c),(d) WBSA, and (e),(f) WBDA (including comparative curves from runoff and WBSA). Values shown are the 38-yr mean and variations (standard deviation) for 1979–2016.

The surface water storage estimated for Mississippi River (Fig. 3b) shows several major differences from that of the WNHB due to its dry and warm climate conditions. First, the magnitude of the surface water storage was small throughout the year and its annual peak value was only 5.3 mm, or 12% of that for the WNHB. The peak time occurred in March, about 3 months earlier than that of the WNHB. Second, zero surface water storage could occur in any month of a year, even during spring snowmelt (March–April). On the other hand, above zero values could even occur in the midwinter months (December–February). Third, the interannual variations were huge relative to its mean values. The CV varied from 130% in March to over 500% in September, October, and January.

The runoff-scaled $(\Delta SW \times A_{MDA})^{2/3}$ surface water areas are compared with Landsat data in Fig. 4. Monthly time series data for five years (2004–08) are presented in order to illustrate the variation details. For WNHB which is located around the latitude of 60°N, Landsat had data for about 5 months (May–September) in a year. For the Mississippi River MDA which is located in latitudes south of 50°N, Landsat data was much improved to 8 months (March–October) in a year.

Landsat-observed water areas showed significant seasonal variations in both WNHB and the Mississippi MDAs. For WNHB (Fig. 4a), Landsat-observed water areas peaked mostly in June and dropped by 5%–10% to its lowest values in August, followed by a substantial increase in September. The interannual variations were found to be relatively small. In comparison, the runoff-scaled areas showed similar patterns as observed in Landsat data; however, two major differences are noticed. 1) The large prewinter rebound observed in the Landsat-based areas was markedly underestimated by the runoff method. 2) The minimum areas from the runoff method mostly appeared in July which was one month earlier than that of Landsat. The water budget of the water body modulated by its hypsometric curve determines the water area dynamics. The above noted differences were mainly

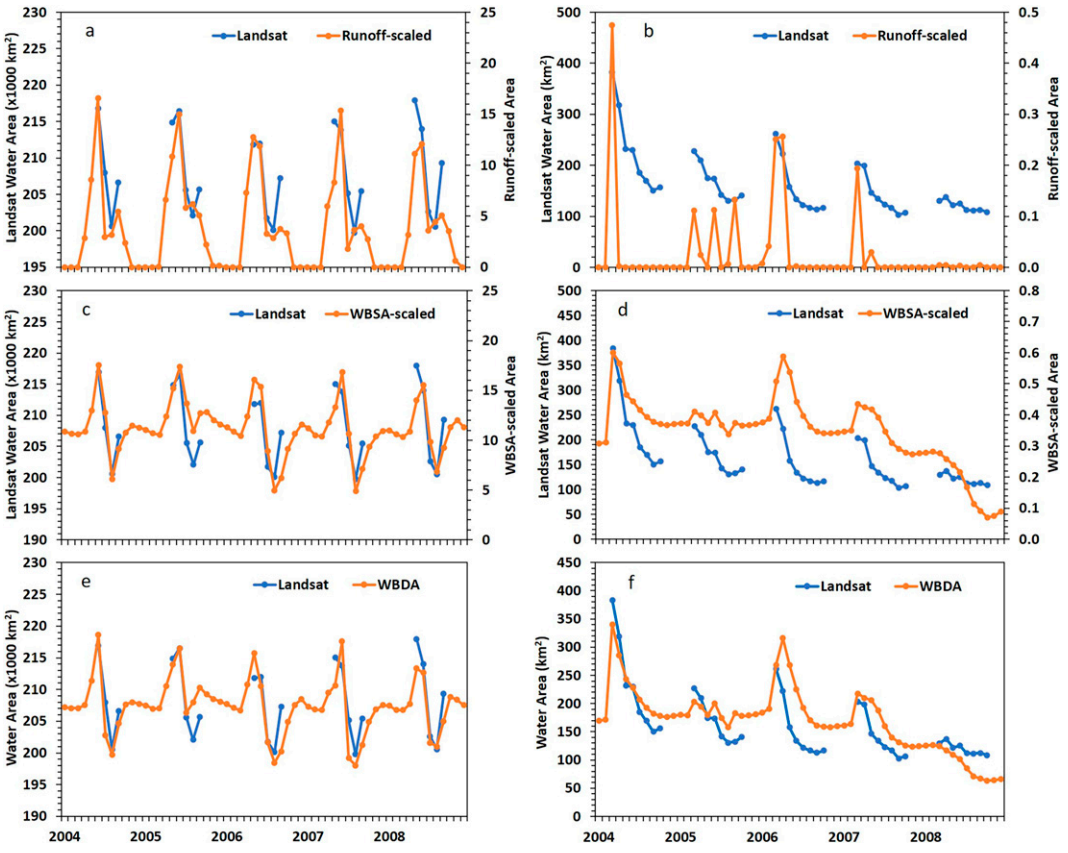


FIG. 4. Comparison of Landsat-observed vs estimated [(a),(b) runoff method, (c),(d) WBSA method, (e),(f) WBDA method] monthly surface water area variations for (left) the Western and North Hudson Bay MDA and (right) the Mississippi River MDA in 2004–08.

caused by the large seasonal variations in water body water yield which the runoff method does not include. This limitation is addressed in the WBSA and WBDA methods detailed below.

For the Mississippi River MDA, comparisons between the Landsat-based and runoff-scaled water areas (Fig. 4b) showed two major differences from that of the WNHB. 1) The seasonal variations of the Landsat-based water areas essentially showed a continuous decrease from March through September. Although a slight prewinter increase in October was noticed, its magnitude was much smaller than the prewinter rebound for the WNHB. The magnitudes of seasonal changes are found to have huge interannual variations. For example, water areas in 2004 dropped as much as 60% from snowmelt season to late summer, but only 20% in 2008. 2) The runoff-scaled area frequently had zero values in a year. In years with dry winter such as 2008, the runoff-scaled areas were essentially zero year-round. The results show that, while the runoff method generally captured the interannual variations as observed by Landsat, it was not able to reproduce the seasonal water variations for this dry MDA. More specifically, land surface runoff cannot have negative values, so the runoff method is unable to deal with the process of continued net water loss (or water area decrease) in dry seasons/years. This limitation is addressed in the WBSA and WBDA methods detailed below.

The overall correlations between Landsat-based and runoff-scaled surface water areas for all the available months for 1990–2016 are given in Fig. 5. The WNHB achieved a fairly high correlation coefficient ($r$) value of 0.720 (Fig. 5a). For the Mississippi River, the $r$ had a relatively low value of 0.572 (Fig. 5b), mainly due to the zero values in summer from the runoff method. It is worth mentioning that among the 11 MDAs, only the Pacific MDA maintained a minimal level of surface runoff year-round. For the 10 other MDAs, zero values of land surface runoff occurred in most winter months due to the frozen land surface conditions.

### *b. Water budget with static water area method*

The results from the WBSA method largely improved the limitations observed with the runoff method:

1) The large prewinter rebound of surface water areas for the WNHB, which was observed by the Landsat data but markedly underestimated by the runoff method as discussed above (Fig. 4a), was successfully reproduced by the WBSA method (Fig. 4c). Further, compared to the runoff method which estimated a dramatic decline in

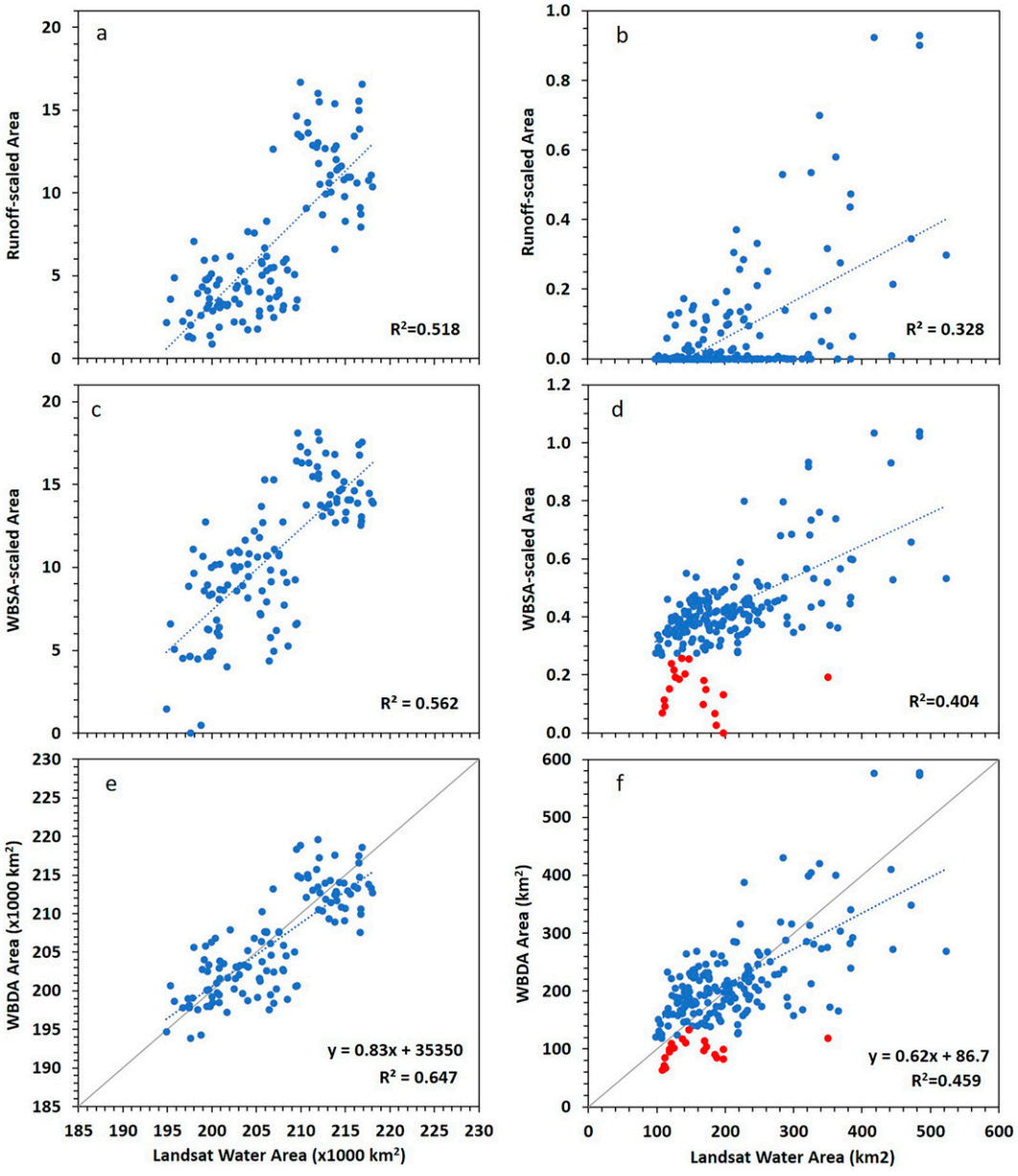


FIG. 5. Correlations between Landsat-observed and estimated [(a),(b) runoff method, (c),(d) WBSA method, (e),(f) WBDA method] surface water areas for (left) the Western and North Hudson Bay MDA and (right) the Mississippi River MDA in 1990–2016. The data points in red represent 19 months from two severe drought periods to be discussed below.

October and remained at zero values throughout the winter season, the WBSA prewinter rebound is continued into November before it started to fall slowly throughout the winter season until March of the next year. This improvement is mainly due to the inclusion of water body water yield in the WBSA method which had an increase in the fall season and a decrease in winter season.

2) The time with annual minimum surface water storage/area for WNHB, which appeared in July in the runoff method (Fig. 3a), was estimated in August by the WBSA method (Fig. 3c) and it agreed with the Landsat observations (Fig. 4c). This difference is mainly due to the impact of high evaporative water loss for the water bodies in August employed in the WBSA method.
3) The seasonal pattern of the surface water storage/area for the Mississippi River shows a continuous decrease from the snowmelt season through January of the next year for the WBSA method (Figs. 3d and 4d), which agreed well with the Landsat observations. It improved the runoff method, which had mostly zero values for the corresponding period

(Figs. 3b and 4b). The September peak obtained with the runoff method (Fig. 3b) was subtle with the WBSA method.

The above changes reported by the WBSA method largely improved the seasonal variation patterns by the runoff method. The correlation coefficient with the Landsat-based surface water areas in 1990–2016 was increased from 0.720 (Fig. 5a) to 0.750 (Fig. 5c) (WNHB), and from 0.572 (Fig. 5b) to 0.636 (Fig. 5d) (Mississippi River) for the runoff and WBSA methods, respectively.

One unique feature found for the Mississippi River MDA is the huge seasonal variations of surface water areas due to its flat terrain and poorly connected hydrological system. An analysis of the Landsat data shows that in the 30 years of 1991–2020, the median and the maximum surface water inundation areas were 120% and 520% of its permanent water area, respectively (Fig. S3). In contrast, for the other 10 MDAs, the median inundation areas were from only 9% (Great Slave Lake MDA) to 27% (Maritime Provinces MDA), and the maximum inundation areas were about 16% and 49% of their corresponding permanent water areas. Another unique feature with the Mississippi River MDA as compared to the other 10 MDAs is that it had a very high surface water evaporation rate (long-term average 984 mm $yr^{-1}$) and low precipitation rate (long-term average 363 mm $yr^{-1}$) which resulted in a negative water body water yield (water loss) of $-621$ mm $yr^{-1}$ (Fig. S4), and very low land surface runoff, or source of water input for water bodies from its surrounding land (12 mm $yr^{-1}$, Fig. S4). In contrast, the other 10 MDAs had much smaller net water loss or even water gain over water body surface, and much higher land surface runoff input (Fig. S4). The WBSA method used a static surface water area for each MDA. The two features mentioned above for Mississippi River suggest that overlooking the water area dynamic variations in the WBSA method could result in large estimation errors for this MDA. This can be confirmed by the lower $r$ value obtained for Mississippi River than that for the WNHB. Additionally, the data points in red (Fig. 5d), which deviated from the general relationship, represent 19 months from two time periods, July 2001 through October 2002, and April 2008 through March 2009 (note that Landsat has no data for November–February for this MDA), which correspond to the two lowest runoff years in our study period after severe climate droughts. Under prolonged drought conditions, using a static surface water area from normal conditions for calculating water body water budgets results in large overestimation of water loss, and vise versa for flooding conditions.

*c. Water budget with dynamic water area method*

The WBDA method addresses the abovementioned shortcomings in the WBSA method. It simulates the dynamic changes of water areas with water storage changes in its water bodies water budget calculations. This leads to a reduction in water areas when water budget is negative during a dry period, and vice versa. It feeds back to the water budget calculations for water bodies. For example, the decrease in water areas under dry conditions leads to the decrease of basin-level evaporative water loss and the increase of total land surface runoff input (due to the increase in land surface areas), and vice versa. Consequently, the WBDA method reduced the seasonal variation amplitude of water storages obtained by the WBSA method (Figs. 3e,f). Overall, we found the seasonal variation patterns by the WBDA and WBSA methods are similar. By comparison, the runoff method shows large errors particularly in the cold season and dry regions.

Another advantage of the WBDA method is that it simulates the actual water areas which makes a direct comparison with the Landsat-based areas possible (Figs. 4e,f). The WBDA method further improved the correlations between the model output and the Landsat data (Figs. 5e,f). In particular, it can be noticed that the months estimated with large errors for the Mississippi River MDA by the WBSA method (the data points in red in Fig. 5d) have been largely corrected (Fig. 5f).

Overall, the runoff, WBSA, and WBDA methods for all the 11 MDAs obtained $r$ values $> 0.5$ with most $r$ values $> 0.7$ (Fig. 6). The differences among the three methods are consistent for each of the MDAs, which show the Runoff method had the lowest $r$ values and the WBDA method achieved the highest $r$ values, demonstrating the improvements made by considering water body water yield in the WBSA method, and by further considering water area dynamics in the WBDA method, in the surface water storage estimation. The three methods performed consistently across the MDAs. High $r$ values were achieved for most of the MDAs, the exceptions being the Nelson River, Yukon River, and Mississippi River. The possible reasons for the relatively low $r$ values for these three MDAs will be discussed next.

## 4. Discussion

Variations among methods and the MDAs with the validation data are considered related to Landsat data (temporal and spatial resolutions) and environmental factors. Three aspects of the MDAs related to physical environments are considered: (i) contribution of glacial melt, (ii) water body connectivity, and (iii) surface water–groundwater connectivity.

Landsat satellites have a revisit frequency of about 2 weeks over the study region. Due to atmospheric contaminations (e.g., clouds) and other missing observations, temporal availability of valid observations for water retrievals are further decreased. This largely limits the number of valid observations for generating monthly water products that well represent the monthly averages, which poses limitations for water characterization over regions where the water area is highly dynamic. This is one reason for the low correlations obtained for the Mississippi River MDA, where water area is highly dynamic. As shown in Fig. S3, the water inundation areas can be 5 times more than its permanent areas for the Mississippi River. This MDA is located in the driest edge of the Canadian Prairies. Its annual water surface evaporation is almost 3 times the amount of precipitation. The land surface of the Canadian Prairies is characterized by the glacier deposits of the Wisconsin glaciation during the Pleistocene era, which left the ground pocked with small depressions known as potholes. Many of

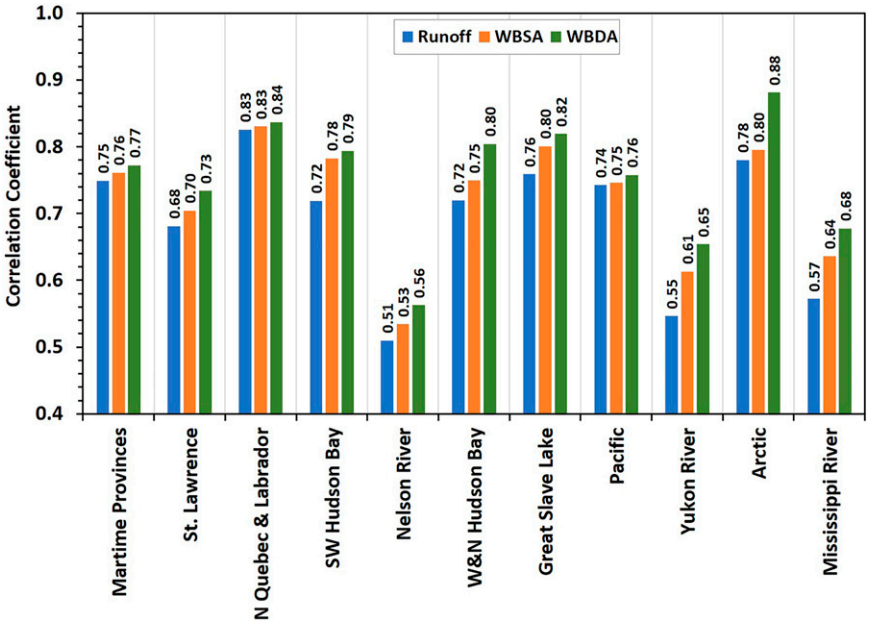


FIG. 6. Correlation coefficients between Landsat-observed surface water areas and the runoff-scaled, WBSA-scaled, and WBDA-simulated surface water areas for the 11 MDAs in Canada.

these potholes are not connected by surface streams. They typically receive most of their water from spring snowmelt to become ponds, wetlands, or sloughs, and often dry up in summer due to high evaporation (Johnson et al. 2005), resulting in highly dynamic water area variations. Integration of multi-satellite missions, particularly those using SAR technologies which can observe Earth's surface in all weather conditions, day and night (e.g., Sentinel-1, RCM), is necessary to obtain high temporal resolution products to improve water monitoring over highly dynamic regions.

Landsat water products have a spatial resolution of 30 m. They have been successfully used in mapping flooding events or long-term (multiyear) water area variations which involve large area changes. For water bodies particularly those with high slope surrounding terrains, the month-over-month shoreline changes outside the time periods with extreme water events (e.g., snowmelt and floods) are often within a few meters, which cannot be accurately detected by Landsat satellites. This relatively coarse spatial resolution poses a challenge in quantifying monthly water variations in many circumstances. It brought up uncertainties in the Landsat monthly water areas and affected our model evaluations. Satellite missions with higher spatial resolution for water surface monitoring (e.g., Sentinel-1/2, *RADARSAT-2*, and RCM), will be used to address the issues in further studies. In particular, the Surface Water and Ocean Topography (SWOT) mission launched in 2022 is expected to greatly advance the surface water studies by providing spatially continuous observations for water area and height information of inland water bodies.

The correlation coefficients for the Yukon River are also relatively low (Fig. 6). This was caused mainly by the large model underestimation in September of each year (note that Landsat data are not available after September for Yukon River). As shown in Fig. S5, Landsat-based water areas had a huge increase in September consistently in each year during our study period, but none of the three methods reproduced this change. By removing the September data, the $r$ value by the WBDA method was increased considerably from 0.654 to 0.843 (Fig. S6). Examination of all the datasets and water processes over this MDA found that there were no meteorological variables that could explain the large change in the Landsat data. On the other hand, the change is highly consistent with the glacier changes reported for the region due to climate change impacts. The Rocky Mountains have an estimated glacierized area of over 38 000 km$^2$ (Ommanney 2002). Wang et al. (2014a, 2015b) reported that the Yukon River basin has experienced significant and consistent water losses in the past four decades due to glacier and permanent snow cover shrinkage. The average water loss rate was reported at a magnitude of 39.5 mm yr$^{-1}$ during 2003–08, with a trend of accelerating loss. Similar results have also been reported in some other studies using satellite and ground observations as well as models over the region (e.g., Spence 2002; Ge et al. 2012; Rodell et al. 2018; Young et al. 2021; Pradhananga and Pomeroy 2022; Wiersma et al. 2022). It is reasonable to assume that the melt of glacier/permanent snow mostly occurs in summer, which provides water input for water bodies and results in surface water area increase in late summer as observed in the Landsat data. This has been observed in other cold regions of the world such as Tibetan Plateau where glacier melt was found to have contributed to water extent increase (Zhang et al. 2011; Zhao et al. 2022). It is worth noting that the precipitation in September over the basin was 25.9 mm, which was only two-thirds of the abovementioned water input

from glacier/permanent-snow melts (39.5 mm). Therefore, the impact of this climate changed–induced water input on surface water areas in late summer is large. The water contribution from this process was not included in the three methods in this study, resulting in the large differences between Landsat data and our estimates in late summer.

The Nelson River showed the lowest $r$ values (Fig. 6) among the 11 MDAs. A large part of the Nelson River MDA belongs to the Canadian Prairies, where the water area is highly dynamic. Glacier and permanent snowmelt in the Rocky Mountains headwater areas of the Nelson River MDA also had significant contribution to its surface water (Comeau et al. 2009), of which the impact on our estimates can be seen in Fig. S5. Additionally, we found that Landsat data showed a significant trend of water area increase over our study period for this MDA (overall trend 290 $km^2$ $yr^{-1}$). Our methods assume that the water bodies in a basin are hydrologically well connected so surplus water can flow out of the system. The unique land surface characteristics over the Canadian Prairie pothole region result in many of the basins over the Nelson River MDA as closed basins (e.g., Winter 1989). This caused discrepancies between Landsat data and our model estimates. After removal of the overall trend from the Landsat data, the correlation coefficient (representing seasonal variations) obtained by the WBDA method was increased to 0.686. It is worth noting that no significant trend was found for the Mississippi River MDA to the south, which suggests that the water increase likely occurred in the northern part of the prairie region. All the above three processes affected the estimates for the Nelson River MDA, which resulted in the lowest correlations with the Landsat observations.

Our methods do not include direct water body–aquifer water exchanges. Groundwater discharge to water bodies in the wet regions with well-connected hydrological systems largely contributes to river baseflow and flows out of the system, so the net change (discharge minus baseflow) and its impact on surface water area is secondary. This can be confirmed by our results which showed fairly high $r$ values for most MDAs except for the prairie dry region. The hydrology over the Canadian Prairies is very variable and complex (Spence et al. 2022). Some potholes may receive groundwater discharge, while some others may be sources for groundwater recharge. However, for the overall prairie region, the impact of groundwater on the water bodies dynamics is secondary to land surface runoff (particularly from snowmelt) and water surface evaporation (Leibowitz and Vining 2003; Johnson et al. 2005; Betts et al. 2014). Nevertheless, direct water body–aquifer water exchange is an additional source of uncertainties affecting our estimates. The surface water–groundwater interactions are complex and data on water body–aquifer water exchanges are extremely rare especially at large scales. Further studies are necessary to couple this process in surface water studies particularly for regions with self-closed hydrological systems.

## 5. Conclusions

Three methods for estimating surface water storage changes are proposed. They include the runoff method, which uses land surface runoff as a proxy for surface water storage; the water budget with static water area (WBSA) method, which calculates surface water budget for water bodies using static water areas; and the dynamic water area simulations (WBDA) based on the WBSA method. The three methods were used to estimate monthly surface water storage changes for 11 major drainage areas (MDAs) that cover Canada's entire landmass. The results were evaluated using observed monthly water areas by the Landsat satellites. The runoff method obtained results with the lowest correlations with the Landsat data. It could have large errors in the estimates in cold season or dry regions. However, it had positive $r$ with moderate values for all the MDAs, indicating it can capture the water variation signal to a certain degree. It suggests that using land surface runoff as a proxy for surface water storage change in GRACE-TWS decomposition provides improvement over the approaches of neglecting this water component. The WBDA method shows the best performance, demonstrating the improvements made by considering water body water yield and water area dynamics in the surface water storage change estimation. The WBDA method, however, needs additional data input for calibrating the surface water volume–area relationships. The WBSA method significantly improved the runoff method, and its estimates had similar seasonal variation patterns to those by the WBDA method. Moreover, the WBSA method is relatively simple. It is thus recommended for surface water storage change estimation when available data are limited for more physically based modeling. The three methods performed consistently across the 11 MDAs. All the methods performed well for most of the MDAs except those that have significant glacier melt input (Yukon, Nelson) and dry regions with poorly connected hydrological system (Mississippi, Nelson). The methods and outputs from this study can be used for calibrating and validating hydrological and climate models, assessing climate change and human disturbance impacts on regional water resources, and filling the ΔSW data gaps in GRACE-based total water storage decompositions studies.

*Acknowledgments.* This study was supported by the Earth Observation for Cumulative Effects (EO4CE) Project of the Natural Resources Canada. The EO4CE project is part of Natural Resources Canada's Status and Trends Program and is funded as a component of the Government of Canada's initiative for the assessment and monitoring of cumulative effects. NRCan contribution number/Numéro de contribution de RNCan: 20220445.

*Data availability statement.* Data used in this study are openly available and can be downloaded from the following links: the Landsat-based Global Surface Water (GSW) Monthly Water History product: https://jeodpp.jrc.ec.europa.eu/ftp/jrc-opendata/GSWE/, Land Surface Runoff and Waterbody Water Yield: ftp://ftp.ccrs.nrcan.gc.ca/ad/EMS/EALCO/.

## REFERENCES

Allen, G. H., C. H. David, K. M. Andreadis, F. Hossain, and J. S. Famiglietti, 2018: Global estimates of river flow wave travel

times and implications for low-latency satellite data. *Geophys. Res. Lett.*, **45**, 7551–7560, https://doi.org/10.1029/2018GL077914.

Bartsch, A., A. M. Trofaier, G. Hayman, D. Sabel, S. Schlaffer, D. B. Clark, and E. Blyth, 2012: Detection of open water dynamics with ENVISAT ASAR in support of land surface modelling at high latitudes. *Biogeosciences*, **9**, 703–714, https://doi.org/10.5194/bg-9-703-2012.

Bergeron, J., G. Siles, R. Leconte, M. Trudel, D. Desroches, and D. L. Peters, 2020: Assessing the capabilities of the Surface Water and Ocean Topography (SWOT) mission for large lake water surface elevation monitoring under different wind conditions. *Hydrol. Earth Syst. Sci.*, **24**, 5985–6000, https://doi.org/10.5194/hess-24-5985-2020.

Betts, A. K., R. Desjardins, D. Worth, S. Wang, and J. Li, 2014: Coupling of winter climate transitions to snow and clouds over the Prairies. *J. Geophys. Res. Atmos.*, **119**, 1118–1139, https://doi.org/10.1002/2013JD021168.

Bhanja, S. N., A. Mukherjee, D. Saha, I. Velicogna, and J. S. Famiglietti, 2016: Validation of GRACE based groundwater storage anomaly using in-situ groundwater level measurements in India. *J. Hydrol.*, **543**, 729–738, https://doi.org/10.1016/j.jhydrol.2016.10.042.

Birkett, C. M., C. Reynolds, B. Beckley, and B. Doorn, 2011: From research to operations: The USDA global reservoir and Lake Monitor. *Coastal Altimetry*, S. Vignudelli et al., Eds., Springer, 19–50, https://doi.org/10.1007/978-3-642-12796-0_2.

Boergens, E., D. Dettmering, C. Schwatke, and F. Seitz, 2016: Treating the hooking effect in satellite altimetry data: A case study along the Mekong River and its tributaries. *Remote Sens.*, **8**, 91, https://doi.org/10.3390/rs8020091.

Bonnema, M., C. H. David, R. P. d. M. Frasson, C. Oaida, and S.-H. Yun, 2022: The global surface area variations of lakes and reservoirs as seen from satellite remote sensing. *Geophys. Res. Lett.*, **49**, e2022GL098987, https://doi.org/10.1029/2022GL098987.

Busker, T., A. d. Roo, E. Gelati, C. Schwatke, M. Adamovic, B. Bisselink, J.-F. Pekel, and A. Cottam, 2019: A global lake and reservoir volume analysis using a surface water dataset and satellite altimetry. *Hydrol. Earth Syst. Sci.*, **23**, 669–690, https://doi.org/10.5194/hess-23-669-2019.

Chen, J., J. S. Famiglietti, B. R. Scanlon, and M. Rodell, 2016: Groundwater storage changes: Present status from GRACE observations. *Surv. Geophys.*, **37**, 397–417, https://doi.org/10.1007/s10712-015-9332-4.

——, J. Liao, and C. Wang, 2021: Improved lake level estimation from radar altimeter using an automatic multiscale-based peak detection retracker. *IEEE J. Sel. Top. Appl. Earth Obs. Remote Sens.*, **14**, 1246–1259, https://doi.org/10.1109/JSTARS.2020.3035686.

Chen, Y., S. Wang, Z. Ren, J. Huang, X. Wang, S. Liu, H. Deng, and W. Lin, 2019: Increased evapotranspiration from land cover changes intensified water crisis in an arid river basin in Northwest China. *J. Hydrol.*, **574**, 383–397, https://doi.org/10.1016/j.jhydrol.2019.04.045.

Comeau, L. E. L., A. Pietroniro, and M. N. Demuth, 2009: Glacier contribution to the North and South Saskatchewan Rivers. *Hydrol. Processes*, **23**, 2640–2653, https://doi.org/10.1002/hyp.7409.

Cooley, S. W., J. C. Ryan, and L. C. Smith, 2021: Human alteration of global surface water storage variability. *Nature*, **591**, 78–81, https://doi.org/10.1038/s41586-021-03262-3.

Crétaux, J.-F., and Coauthors, 2011: SOLS: A lake database to monitor in the near real time water level and storage variations from remote sensing data. *Adv. Space Res.*, **47**, 1497–1507, https://doi.org/10.1016/j.asr.2011.01.004.

Downing, J. A., 2010: Emerging global role of small lakes and ponds: Little things mean a lot. *Limnetica*, **1**, 9–24, https://doi.org/10.23818/limn.29.02.

——, and Coauthors, 2006: The global abundance and size distribution of lakes, ponds, and impoundments. *Limnol. Oceanogr.*, **51**, 2388–2397, https://doi.org/10.4319/lo.2006.51.5.2388.

Famiglietti, J. S., 2014: The global groundwater crisis. *Nat. Climate Change*, **4**, 945–948, https://doi.org/10.1038/nclimate2425.

——, and G. Ferguson, 2021: The hidden crisis beneath our feet: Disappearing groundwater requires action to prevent widespread water scarcity. *Science*, **372**, 344–345, https://doi.org/10.1126/science.abh2867.

Fatolazadeh, F., and K. Goïta, 2022: Reconstructing groundwater storage variations from GRACE observations using a new Gaussian-Han-Fan (GHF) smoothing approach. *J. Hydrol.*, **604**, 127234, https://doi.org/10.1016/j.jhydrol.2021.127234.

Fernandes, R., V. Korolevich, and S. Wang, 2007: Trends in land evapotranspiration over Canada for the period 1960–2000 based on in situ climate observations and a land surface model. *J. Hydrometeor.*, **8**, 1016–1030, https://doi.org/10.1175/JHM619.1.

Frappart, F., S. Calmant, M. Cauhopé, F. Seyler, and A. Cazenave, 2006: Preliminary results of ENVISAT RA-2-derived water levels validation over the Amazon basin. *Remote Sens. Environ.*, **100**, 252–264, https://doi.org/10.1016/j.rse.2005.10.027.

Ge, S., D. Yang, and D. L. Kane, 2012: Yukon River basin long-term (1977–2006) hydrologic and climatic analysis. *Hydrol. Processes*, **27**, 2475–2484, https://doi.org/10.1002/hyp.9282.

Getirana, A., S. Kumar, M. Girotto, and M. Rodell, 2017: Rivers and floodplains as key components of global terrestrial water storage variability. *Geophys. Res. Lett.*, **44**, 10 359–10 368, https://doi.org/10.1002/2017GL074684.

Grant, R. F., and Coauthors, 2006: Intercomparison of techniques to model water stress effects on $CO_2$ and energy exchange in temperate and boreal deciduous forests. *Ecol. Modell.*, **196**, 289–312, https://doi.org/10.1016/j.ecolmodel.2006.02.035.

Hanson, P. J., and Coauthors, 2004: Oak forest carbon and water simulations: Model intercomparisons and evaluations against independent data. *Ecol. Monogr.*, **74**, 443–489, https://doi.org/10.1890/03-4049.

Hou, J., A. I. J. M. van Dijk, H. E. Beck, L. J. Renzullo, and Y. Wada, 2022: Remotely sensed reservoir water storage dynamics (1984–2015) and the influence of climate variability and management at a global scale. *Hydrol. Earth Syst. Sci.*, **26**, 3785–3803, https://doi.org/10.5194/hess-26-3785-2022.

Huang, W., B. DeVries, C. Huang, M. W. Lang, J. W. Jones, I. F. Creed, and M. L. Carroll, 2018: Automated extraction of surface water extent from Sentinel-1 data. *Remote Sens.*, **10**, 797, https://doi.org/10.3390/rs10050797.

Johnson, W. C., B. V. Millett, T. Gilmanov, R. A. Voldseth, G. R. Guntenspergen, and D. E. Naugle, 2005: Vulnerability of Northern Prairie wetlands to climate change. *BioScience*, **55**, 863, https://doi.org/10.1641/0006-3568(2005)055[0863:VONPWT]2.0.CO;2.

Jones, J. W., 2019: Improved automated detection of subpixel-scale inundation—Revised dynamic surface water extent (DSWE) partial surface water tests. *Remote Sens.*, **11**, 374, https://doi.org/10.3390/rs11040374.

Joodaki, G., J. Wahr, and S. Swenson, 2014: Estimating the human contribution to groundwater depletion in the Middle East, from GRACE data, land surface models, and well observations. *Water Resour. Res.*, **50**, 2679–2692, https://doi.org/10.1002/2013WR014633.

Khandelwal, A., A. Karpatne, M. E. Marlier, J. Kim, D. P. Lettenmaier, and V. Kumar, 2017: An approach for global monitoring of surface water extent variations in reservoirs using MODIS data. *Remote Sens. Environ.*, **202**, 113–128, https://doi.org/10.1016/j.rse.2017.05.039.

Kim, H., P. J.-F. Yeh, T. Oki, and S. Kanae, 2009: Role of rivers in the seasonal variations of terrestrial water storage over global basins. *Geophys. Res. Lett.*, **36**, L17402, https://doi.org/10.1029/2009GL039006.

Landerer, F. W., and Coauthors, 2020: Extending the global mass change data record: GRACE Follow-On instrument and science data performance. *Geophys. Res. Lett.*, **47**, e2020GL088306, https://doi.org/10.1029/2020GL088306.

Lehner, B., and P. Döll, 2004: Development and validation of a global database of lakes, reservoirs and wetlands. *J. Hydrol.*, **296**, 1–22, https://doi.org/10.1016/j.jhydrol.2004.03.028.

Leibowitz, S. G., and K. C. Vining, 2003: Temporal connectivity in a prairie pothole complex. *Wetlands*, **23**, 13–25, https://doi.org/10.1672/0277-5212(2003)023[0013:TCIAPP]2.0.CO;2.

Li, J., and S. Wang, 2015: An automatic method for mapping inland surface water bodies with Radarsat-2 imagery. *Int. J. Remote Sens.*, **36**, 1367–1384, https://doi.org/10.1080/01431161.2015.1009653.

——, and ——, 2022: Seasonal variations and long-term trends of groundwater over the Canadian landmass. *Hydrogeol. J.*, **30**, 401–415, https://doi.org/10.1007/s10040-022-02460-1.

——, ——, and F. Zhou, 2016: Time series analysis of long-term terrestrial water storage over Canada from GRACE satellites using principal component analysis. *Can. J. Remote Sens.*, **42**, 161–170, https://doi.org/10.1080/07038992.2016.1166042.

Li, X., D. Long, Q. Huang, P. Han, F. Zhao, and Y. Wada, 2019: High-temporal-resolution water level and storage change data sets for lakes on the Tibetan Plateau during 2000–2017 using multiple altimetric missions and Landsat-derived lake shoreline positions. *Earth Syst. Sci. Data*, **11**, 1603–1627, https://doi.org/10.5194/essd-11-1603-2019.

Li, Z., and S. Wang, 2021: Water yield variability and response to climate change across Canada. *Hydrol. Sci. J.*, **66**, 1169–1184, https://doi.org/10.1080/02626667.2021.1925122.

——, ——, and J. Li, 2020: Spatial variations and long-term trends of potential evaporation in Canada. *Sci. Rep.*, **10**, 22089, https://doi.org/10.1038/s41598-020-78994-9.

Long, D., L. Longuevergne, and B. R. Scanlon, 2015: Global analysis of approaches for deriving total water storage changes from GRACE satellites. *Water Resour. Res.*, **51**, 2574–2594, https://doi.org/10.1002/2014WR016853.

——, and Coauthors, 2020: South-to-north water diversion stabilizing Beijing's groundwater levels. *Nat. Commun.*, **11**, 3665, https://doi.org/10.1038/s41467-020-17428-6.

Luo, S., and Coauthors, 2022: Satellite laser altimetry reveals a net water mass gain in global lakes with spatial heterogeneity in the early 21st century. *Geophys. Res. Lett.*, **49**, e2021GL096676, https://doi.org/10.1029/2021GL096676.

McDonald, C. P., J. A. Rover, E. G. Stets, and R. G. Striegl, 2012: The regional abundance and size distribution of lakes and reservoirs in the United States and implications for estimates of global lake extent. *Limnol. Oceanogr.*, **57**, 597–606, https://doi.org/10.4319/lo.2012.57.2.0597.

Medlyn, B. E., and Coauthors, 2015: Using ecosystem experiments to improve vegetation models. *Nat. Climate Change*, **5**, 528–534, https://doi.org/10.1038/nclimate2621.

Messager, M. L., B. Lehner, G. Grill, I. Nedeva, and O. Schmitt, 2016: Estimating the volume and age of water stored in global lakes using a geo-statistical approach. *Nat. Commun.*, **7**, 13603, https://doi.org/10.1038/ncomms13603.

Minns, C. K., J. E. Moore, B. J. Shuter, and N. E. Mandrak, 2008: A Preliminary national analysis of some key characteristics of Canadian lakes. *Can. J. Fish. Aquat. Sci.*, **65**, 1763–1778, https://doi.org/10.1139/F08-110.

Normandin, C., F. Frappart, B. Lubac, S. Bélanger, V. Marieu, F. Blarel, A. Robinet, and L. Guiastrennec-Faugas, 2018: Quantification of surface water volume changes in the Mackenzie Delta using satellite multi-mission data. *Hydrol. Earth Syst. Sci.*, **22**, 1543–1561, https://doi.org/10.5194/hess-22-1543-2018.

Ogilvie, A., G. Belaud, S. Massuel, M. Mulligan, P. Le Goulven, and R. Calvez, 2018: Surface water monitoring in small water bodies: Potential and limits of multi-sensor Landsat time series. *Hydrol. Earth Syst. Sci.*, **22**, 4349–4380, https://doi.org/10.5194/hess-22-4349-2018.

Ommanney, C. S. L., 2002: Glaciers of Canada: Canadian Rockies. Satellite Image Atlas of Glaciers of the World, R. S. Williams Jr. and J. G. Ferrigno, Eds., U.S. Geological Survey Professional Paper 1386-J-1, https://pubs.usgs.gov/pp/p1386j/.

Papa, F., C. Prigent, F. Aires, C. Jimenez, W. B. Rossow, and E. Matthews, 2010: Interannual variability of surface water extent at the global scale, 1993–2004. *J. Geophys. Res.*, **115**, D12111, https://doi.org/10.1029/2009JD012674.

——, F. Frappart, A. Güntner, C. Prigent, F. Aires, A. C. V. Getirana, and R. Maurer, 2013: Surface freshwater storage and variability in the Amazon basin from multi-satellite observations, 1993–2007. *J. Geophys. Res. Atmos.*, **118**, 11 951–11 965, https://doi.org/10.1002/2013JD020500.

Pekel, J.-F., A. Cottam, N. Gorelick, and A. S. Belward, 2016: High-resolution mapping of global surface water and its long-term changes. *Nature*, **540**, 418–422, https://doi.org/10.1038/nature20584.

Pickens, A. H., M. C. Hansen, M. Hancher, S. V. Stehman, A. Tyukavina, P. Potapov, B. Marroquin, and Z. Sherani, 2020: Mapping and sampling to characterize global inland water dynamics from 1999 to 2018 with full Landsat time-series. *Remote Sens. Environ.*, **243**, 111792, https://doi.org/10.1016/j.rse.2020.111792.

Pokhrel, Y. N., Y. Fan, G. Miguez-Macho, P. J.-F. Yeh, and S.-C. Han, 2013: The role of groundwater in the Amazon water cycle: 3. Influence on terrestrial water storage computations and comparison with GRACE. *J. Geophys. Res. Atmos.*, **118**, 3233–3244, https://doi.org/10.1002/jgrd.50335.

Pradhananga, D., and J. W. Pomeroy, 2022: Recent hydrological response of glaciers in the Canadian Rockies to changing climate and glacier configuration. *Hydrol. Earth Syst. Sci.*, **26**, 2605–2616, https://doi.org/10.5194/hess-26-2605-2022.

Prigent, C., F. Papa, F. Aires, W. B. Rossow, and E. Matthews, 2007: Global inundation dynamics inferred from multiple satellite observations, 1993–2000. *J. Geophys. Res.*, **112**, D12107, https://doi.org/10.1029/2006JD007847.

Rateb, A., and Coauthors, 2020: Comparison of groundwater storage changes from GRACE satellites with monitoring and modeling of major U.S. aquifers. *Water Resour. Res.*, **56**, e2020WR027556, https://doi.org/10.1029/2020WR027556.

Richey, A. S., B. F. Thomas, M.-H. Lo, J. T. Reager, J. S. Famiglietti, K. Voss, S. Swenson, and M. Rodell, 2015: Quantifying

renewable groundwater stress with GRACE. *Water Resour. Res.*, **51**, 5217–5238, https://doi.org/10.1002/2015WR017349.

Rodell, M., and Coauthors, 2004: The Global Land Data Assimilation System. *Bull. Amer. Meteor. Soc.*, **85**, 381–394, https://doi.org/10.1175/BAMS-85-3-381.

——, J. Chen, H. Kato, J. S. Famiglietti, J. Nigro, and C. R. Wilson, 2007: Estimating groundwater storage changes in the Mississippi River basin (USA) using GRACE. *Hydrogeol. J.*, **15**, 159–166, https://doi.org/10.1007/s10040-006-0103-7.

——, I. Velicogna, and J. S. Famiglietti, 2009: Satellite-based estimates of groundwater depletion in India. *Nature*, **460**, 999–1002, https://doi.org/10.1038/nature08238.

——, J. S. Famiglietti, D. N. Wiese, J. T. Reager, H. K. Beaudoing, F. W. Landerer, and M.-H. Lo, 2018: Emerging trends in global freshwater availability. *Nature*, **557**, 651–659, https://doi.org/10.1038/s41586-018-0123-1.

Salameh, E., and Coauthors, 2017: Fifteen years (1993–2007) of surface freshwater storage variability in the Ganges-Brahmaputra River Basin using multi-satellite observations. *Water*, **9**, 245, https://doi.org/10.3390/w9040245.

Scanlon, B. R., L. Longuevergne, and D. Long, 2012: Ground referencing GRACE satellite estimates of groundwater storage changes in the California Central Valley, USA. *Water Resour. Res.*, **48**, W04520, https://doi.org/10.1029/2011WR011312.

——, and Coauthors, 2019: Tracking seasonal fluctuations in land water storage using global models and GRACE satellites. *Geophys. Res. Lett.*, **46**, 5254–5264, https://doi.org/10.1029/2018GL081836.

——, A. Rateb, D. R. Pool, W. Sanford, H. Save, A. Sun, D. Long, and B. Fuchs, 2021: Effects of climate and irrigation on GRACE-based estimates of water storage changes in major US aquifers. *Environ. Res. Lett.*, **16**, 094009, https://doi.org/10.1088/1748-9326/ac16ff.

Schwatke, C., D. Dettmering, W. Bosch, and F. Seitz, 2015: DAHITI–An innovative approach for estimating water level time series over inland waters using multi-mission satellite altimetry. *Hydrol. Earth Syst. Sci.*, **19**, 4345–4364, https://doi.org/10.5194/hess-19-4345-2015.

Shamsudduha, M., and R. G. Taylor, 2020: Groundwater storage dynamics in the world's large aquifer systems from GRACE: Uncertainty and role of extreme precipitation. *Earth Syst. Dyn.*, **11**, 755–774, https://doi.org/10.5194/esd-11-755-2020.

Sheffield, J., G. Goteti, and E. F. Wood, 2006: Development of a 50-yr high-resolution global dataset of meteorological forcings for land surface modeling. *J. Climate*, **19**, 3088–3111, https://doi.org/10.1175/JCLI3790.1.

Shu, S., and Coauthors, 2020: Analysis of Sentinel-3 SAR altimetry waveform retracking algorithms for deriving temporally consistent water levels over ice-covered lakes. *Remote Sens. Environ.*, **239**, 111643, https://doi.org/10.1016/j.rse.2020.111643.

Smith, S. V., W. H. Renwick, J. D. Bartley, and R. W. Buddemeier, 2002: Distribution and significance of small, artificial water bodies across the United States landscape. *Sci. Total Environ.*, **299**, 21–36, https://doi.org/10.1016/S0048-9697(02)00222-X.

Spence, C., 2002: Streamflow variability (1965 to 1998) in five Northwest Territories and Nunavut Rivers. *Can. Water Resour. J.*, **27**, 135–154, https://doi.org/10.4296/cwrj2702135.

——, Z. He, K. R. Shook, J. W. Pomeroy, C. J. Whitfield, and J. D. Wolfe, 2022: Assessing runoff sensitivity of North American Prairie Pothole Region basins to wetland drainage using a basin classification–based virtual modeling approach. *Hydrol. Earth Syst. Sci.*, **26**, 5555–5575, https://doi.org/10.5194/hess-26-5555-2022.

Statistics Canada, 2003: Standard Drainage Area Classification (SDAC) 2003. Statistics Canada, https://www.statcan.gc.ca/en/subjects/standard/sdac/sdacinfo1.

Tapley, B. D., S. Bettadpur, M. Watkins, and C. Reigber, 2004: The gravity recovery and climate experiment: Mission overview and early results. *Geophys. Res. Lett.*, **31**, L09607, https://doi.org/10.1029/2004GL019920.

Thomas, B. F., J. Caineta, and J. Nanteza, 2017: Global assessment of groundwater sustainability based on storage anomalies. *Geophys. Res. Lett.*, **44**, 11 445–11 455, https://doi.org/10.1002/2017GL076005.

Tiwari, V. M., J. Wahr, and S. Swenson, 2009: Dwindling groundwater resources in northern India, from satellite gravity observations. *Geophys. Res. Lett.*, **36**, L18401, https://doi.org/10.1029/2009GL039401.

Tulbure, M. G., and M. Broich, 2013: Spatiotemporal dynamic of surface water bodies using Landsat time-series data from 1999 to 2011. *ISPRS J. Photogramm. Remote Sens.*, **79**, 44–52, https://doi.org/10.1016/j.isprsjprs.2013.01.010.

Verpoorter, C., T. Kutser, D. A. Seekell, and L. J. Tranvik, 2014: A global inventory of lakes based on high-resolution satellite imagery. *Geophys. Res. Lett.*, **41**, 6396–6402, https://doi.org/10.1002/2014GL060641.

Voss, K. A., J. S. Famiglietti, M. Lo, C. de Linage, M. Rodell, and S. C. Swenson, 2013: Groundwater depletion in the Middle East from GRACE with implications for transboundary water management in the Tigris-Euphrates-Western Iran region. *Water Resour. Res.*, **49**, 904–914, https://doi.org/10.1002/wrcr.20078.

Walker, A. P., and Coauthors, 2014: Comprehensive ecosystem model-data synthesis using multiple data sets at two temperate forest free-air $CO_2$ enrichment experiments: Model performance at ambient $CO_2$ concentration. *J. Geophys. Res. Biogeosci.*, **119**, 937–964, https://doi.org/10.1002/2013JG002553.

Wang, S., 2008: Simulation of evapotranspiration and its response to plant water and $CO_2$ transfer dynamics. *J. Hydrometeor.*, **9**, 426–443, https://doi.org/10.1175/2007JHM918.1.

——, and J. Li, 2016: Terrestrial water storage climatology for Canada from GRACE satellite observations in 2002–2014. *Can. J. Rem. Sens.*, **42**, 190–202, https://doi.org/10.1080/07038992.2016.1171132.

——, and H. A. J. Russell, 2016: Forecasting snowmelt-induced flooding using GRACE satellite data: A case study for the Red River Watershed. *Can. J. Rem. Sens.*, **42**, 203–213, https://doi.org/10.1080/07038992.2016.1171132.

——, R. F. Grant, D. L. Verseghy, and T. A. Black, 2002: Modelling carbon dynamics of boreal forest ecosystems using the Canadian Land surface scheme. *Climatic Change*, **55**, 451–477, https://doi.org/10.1023/A:1020780211008.

——, A. P. Trishchenko, and X. Sun, 2007: Simulation of canopy radiation transfer and surface albedo in the EALCO model. *Climate Dyn.*, **29**, 615–632, https://doi.org/10.1007/s00382-007-0252-y.

——, Y. Yang, A. P. Trishchenko, A. G. Barr, T. A. Black, and H. McCaughey, 2009: Modelling the response of canopy stomatal conductance to humidity. *J. Hydrometeor.*, **10**, 521–532, https://doi.org/10.1175/2008JHM1050.1.

——, ——, Y. Luo, and A. Rivera, 2013: Spatial and seasonal variations in evapotranspiration over Canada's landmass. *Hydrol. Earth Syst. Sci.*, **17**, 3561–3575, https://doi.org/10.5194/hess-17-3561-2013.

——, J. Huang, J. Li, A. Rivera, D. W. McKenney, and J. Sheffield, 2014a: Assessment of water budget for sixteen large drainage

basins in Canada. *J. Hydrol.*, **512**, 1–15, https://doi.org/10.1016/j.jhydrol.2014.02.058.

——, D. W. McKenney, J. Shang, and J. Li, 2014b: A national scale assessment of long-term water budget closures for Canada's watersheds. *J. Geophys. Res. Atmos.*, **119**, 8712–8725, https://doi.org/10.1002/2014JD021951.

——, and Coauthors, 2015a: Comparing evapotranspiration from eddy covariance measurements, water budgets, remote sensing, and land surface models over Canada. *J. Hydrometeor.*, **16**, 1540–1560, https://doi.org/10.1175/JHM-D-14-0189.1.

——, J. Huang, D. Yang, G. Pavlic, and J. Li, 2015b: Long-term water budget imbalances and error sources for cold region drainage basins. *Hydrol. Processes*, **29**, 2125–2136, https://doi.org/10.1002/hyp.10343.

——, F. Zhou, and H. A. J. Russell, 2017: Estimating snow mass and peak river flows for the Mackenzie River basin using GRACE satellite observations. *Remote Sens.*, **9**, 256, https://doi.org/10.3390/rs9030256.

Wang, X., and Coauthors, 2020: Gainers and losers of surface and terrestrial water resources in China during 1989–2016. *Nat. Commun.*, **11**, 3471, https://doi.org/10.1038/s41467-020-17103-w.

Wiersma, P., J. Aerts, H. Zekollari, M. Hrachowitz, N. Drost, M. Huss, E. H. Sutanudjaja, and R. Hut, 2022: Coupling a global glacier model to a global hydrological model prevents underestimation of glacier runoff. *Hydrol. Earth Syst. Sci.*, **26**, 5971–5986, https://doi.org/10.5194/hess-26-5971-2022.

Winter, T. C., 1989: Hydrologic studies of wetlands in the northern prairie. *Northern Prairie Wetlands*, Iowa State University Press, 16–54.

Xia, Y. L., D. Mocko, M. Huang, B. Li, M. Rodell, K. E. Mitchell, X. Cai, and M. B. Ek, 2017: Comparison and assessment of three advanced land surface models in simulating terrestrial water storage components over the United States. *J. Hydrometeor.*, **18**, 625–649, https://doi.org/10.1175/JHM-D-16-0112.1.

Yao, F., J. Wang, C. Wang, and J.-F. Crétaux, 2019: Constructing long-term high-frequency time series of global lake and reservoir areas using Landsat imagery. *Remote Sens. Environ.*, **232**, 111210, https://doi.org/10.1016/j.rse.2019.111210.

Young, J. C., E. Pettit, A. Arendt, E. Hood, G.E. Liston, and J. Beamer, 2021: A changing hydrological regime: Trends in magnitude and timing of glacier ice melt and glacier runoff in a high latitude coastal watershed. *Water Resour. Res.*, **57**, e2020WR027404, https://doi.org/10.1029/2020WR027404.

Zhang, G., H. Xie, S. Kang, D. Yi, and S. F. Ackley, 2011: Monitoring lake level changes on the Tibetan Plateau using ICESat altimetry data (2003–2009). *Remote Sens. Environ.*, **115**, 1733–1742, https://doi.org/10.1016/j.rse.2011.03.005.

Zhang, Y., S. Wang, A. G. Barr, and T. A. Black, 2008: Impact of snow cover on soil temperature and its simulation in a boreal aspen forest. *Cold Reg. Sci. Technol.*, **52**, 355–370, https://doi.org/10.1016/j.coldregions.2007.07.001.

Zhao, F., D. Long, X. Li, Q. Huang, and P. Han, 2022: Rapid glacier mass loss in the southeastern Tibetan Plateau since the year 2000 from satellite observations. *Remote Sens. Environ.*, **270**, 112853, https://doi.org/10.1016/j.rse.2021.112853.

Zhao, G., and H. Gao, 2018: Automatic correction of contaminated images for assessment of reservoir surface area dynamics. *Geophys. Res. Lett.*, **45**, 6092–6099, https://doi.org/10.1029/2018GL078343.

Zou, Z., X. Xiao, J. Dong, Y. Qin, R. B. Doughty, M. A. Menarguez, G. Zhang, and J. Wang, 2018: Divergent trends of open-surface water body area in the contiguous United States from 1984 to 2016. *Proc. Natl. Acad. Sci. USA*, **115**, 3810–3815, https://doi.org/10.1073/pnas.1719275115.